# Residual stress preserved in quartz from the San Andreas Fault Observatory at Depth

Kai Chen[1], Martin Kunz[2], Nobumichi Tamura[2], and Hans-Rudolf Wenk[3]
[1]Center for Advancing Materials Performance from the Nanoscale (CAMP-Nano), State Key Laboratory for Mechanical Behavior of Materials, Xi'an Jiantong University, Xi'an, Shaanxi 710049, China
[2]Advanced Light Source, Lawrence Berkeley National Laboratory, Berkeley, California 94720, USA
[3]Earth and Planetary Science, University of California–Berkeley, Berkeley, California 94720, USA

## ABSTRACT

**We report on measurements of residual stress up to 300 MPa with a microfocused synchrotron X-ray beam in quartz fragments in a cataclasite from the damage zone of the San Andreas fault, California (USA). Samples were extracted from the San Andreas Fault Observatory at Depth drill core at a depth of 2.7 km. Stresses were derived from lattice distortions observed on Laue diffraction images. These stresses are distributed nonhomogeneously at the micron scale and are much higher than bulk-rock strengths of fault gouge, suggesting different processes at the microscopic and macroscopic scales. Our results indicate that residual lattice strain in quartz is a potential paleopiezometer to estimate stress in deformed rocks.**

## INTRODUCTION

Stresses that are released during earthquakes have been of major interest in seismology, engineering, structural geology, and mineral physics (Byerlee, 1978; van der Elst and Brodsky, 2010). In an effort to better understand earthquake mechanisms, several deep drilling projects have been undertaken to retrieve material from seismically active zones of major faults, such as the San Andreas Fault Observatory at Depth (SAFOD) for the San Andreas fault in California (Zoback et al., 2011), the Nojima fault in Japan (Ohtani et al., 2000), the Taiwan Chelungpu-Fault Drilling Project (Ma et al., 2006), the Deep Fault Drilling Project for the Alpine fault in New Zealand (Townend et al., 2009), the Wenchuan earthquake Fault Scientific Drilling Project in China (Xue et al., 2013), and the Japan Trench Fast Drilling Project for the plate boundary thrust off the coast of Japan (Chester et al., 2013). Material retrieved from drill cores can be studied in the laboratory and thus provides direct information about physical and chemical processes that occur at depth within a seismically active zone. Data obtained from such projects can then be compared with records of active seismicity to advance our understanding of the way different mechanisms of brittle failure in Earth's crust are recorded at microscopic to macroscopic scales and how these influence the type of earthquake produced.

Of particular interest from a rock mechanics point of view is fault gouge formed during seismic displacements. Fault gouge is composed of mineral fragments, typically including quartz, feldspar, and phyllosilicates resulting from comminution and alteration reactions. Some of the phyllosilicates are authigenic, suggesting an environment with aqueous components (Gratier et al., 2011; Janssen et al., 2012). In SAFOD material we also find extensively fractured quartz cataclasites, such as the sample studied here (hole E, run 1, section 6, Dressen, at 3141 m; www.earthscope.org/science/data/data-access/safod-data/) that stems from the Great Valley Formation in the damage zone, ~50 m from the currently active southwest deforming zone (e.g., Zoback et al., 2011, their figures 3 and 5). Because the shear strength of quartz at low temperature and pressure is between 4 and 10 GPa (LaLone and Gupta, 2009), rocks containing fractured quartz grains must have undergone such high stresses at least locally. This optical evidence of brittle failure of quartz grains raises the question whether some residual stresses connected to the stress field causing the brittle failure are still preserved in the crystal lattice.

In this study we used synchrotron X-ray Laue microdiffraction as a probe to measure residual deviatoric lattice strain with a high spatial resolution (<1 µm). Laue microdiffraction was developed by materials scientists to characterize texture, strain, and stress on a subgrain level (e.g., Chen et al., 2009; Ice et al., 2011; Jiang et al., 2013). Residual stress has been investigated in metals for a long time, documenting lattice distortions through diffraction evidence (e.g., Noyan and Cohen, 1987). Here we present a first application of this powerful technique to investigate residual stress in quartz from an active earthquake zone.

## METHODS

### Elastic and Plastic Strain

The shape change of a crystalline solid can be elastic strain or plastic strain. Elastic strain in crystals is expressed as a distortion of the crystal lattice. This changes length and angles between lattice vectors, which can be experimentally observed in shifts of the position of X-ray diffraction peaks. For example, in a strained cubic crystal the three equivalent lattice parameters are no longer the same. Plastic strain in crystals is generally achieved by creation and migration of dislocations, causing bending of lattice planes, and results in broadening of diffraction peaks. Plastic strain is preserved but elastic strain is generally reversed when the stress is removed. However, some elastic strain may be trapped inside crystals because their strain state is confined by adjacent grains or defects, resulting in local residual stress (for more details about residual stress see Section 1 in the GSA Data Repository[1]).

### Laue X-Ray Microdiffraction

A thin section was prepared by mounting a slab with epoxy on a glass slide and grinding it to 30 µm. Under a petrographic microscope with crossed polarizers, the section shows two fractured quartz grains with fractures partially filled by calcite veins (Fig. 1A). These grains are embedded in a more fine-grained matrix consisting of quartz, feldspar, and phyllosilicates.

The experiments were conducted at Beamline 12.3.2 of the Advanced Light Source (ALS) at Lawrence Berkeley National Laboratory (Berkeley, California; Kunz et al., 2009). A polychromatic X-ray beam (5–24 keV) was focused to ~1 × 1 µm$^2$ by a pair of Kirkpatrick-Baez mirrors. The sample was mounted on a high-resolution x-y scan stage and tilted 45° relative to the incident X-ray beam. Laue diffraction images (Fig. 2) were recorded in reflection mode with a two-dimensional Pilatus-1M detector mounted at 90° to the incoming X-ray, ~140 mm from the probe spot (Fig. 2, inset). Exposure time at each position was 1 s. The sharp reflections indicate a relatively small amount of plastic deformation and therefore low dislocation density within the probed diffraction volume (~1 × 1 × 40 µm$^3$). Peak positions are determined by fitting of a two-dimensional Gaussian function, providing an angular resolution of ~0.01°. We performed four scans on thee quartz grains on areas ranging from 320 × 240 µm$^2$ to 400 ×

[1]GSA Data Repository item 2015077, supplementary materials on type and origin of residual stresses, measurement of strain/stress tensors, and details of scans, comparing synthetic quartz crystal with four scans of quartz from SAFOD sample, is available online at www.geosociety.org/pubs/ft2015.htm, or on request from editing@geosociety.org or Documents Secretary, GSA, P.O. Box 9140, Boulder, CO 80301, USA.

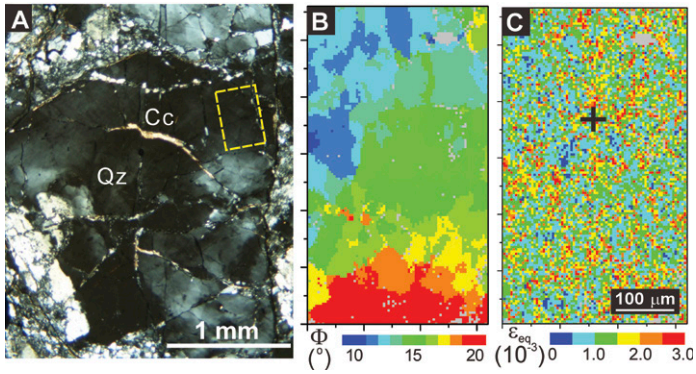


**Figure 1. A: Optical micrograph under crossed polarizers of gouge investigated in this study (from the San Andreas Fault Observatory at Depth). Highly fractured quartz grains with variable extinction on a millimeter scale are embedded in a fine-grained matrix consisting of quartz, feldspar, and phyllosilicates (Qz—large quartz grain, Cc—calcite vein). B: Map of Euler angle Φ that defines the tilt of the crystal c-axis relative to the sample surface. Map is derived from this Laue microdiffraction experiment. C: Map of equivalent strain (in $10^{-3}$ units). Black cross refers to the position where the Laue pattern depicted in Figure 2 was exposed.**

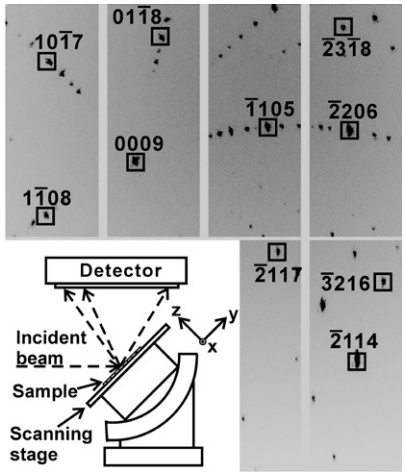


**Figure 2. Laue diffraction image of quartz crystal from gouge zone investigated in this study (from the San Andreas Fault Observatory at Depth). Note the sharp reflections, indicating a low dislocation density within the diffraction volume probed. This pattern was collected on the spot indicated by the cross in Figure 1C and corresponds to a residual stress of 300 MPa. Inset shows a sketch of the experimental set up; the sample is placed at 45° relative to the incoming beam.**

600 μm². Step size was 4 μm. For comparison, a scan was performed on a thin section of a synthetic quartz crystal prepared and analyzed using the same methodology as for the SAFOD sample.

### Data Analysis

All diffraction patterns (between 4800 and 15000 frames per scan) were analyzed automatically by the software package XMAS (Tamura, 2014). The analysis is performed by indexing each individual pattern to determine the relative orientation of the crystal lattice. The trigonality of quartz is resolved by taking into account the observed diffraction intensities (Chen et al., 2012). The difference between the observed reflection positions and those calculated based on the assumption of an unstrained lattice are used to calculate the deviatoric strain tensor $\varepsilon'$ ($\varepsilon' = \varepsilon_{tot} - \delta$, where $\varepsilon_{tot}$ is total strain, and $\delta$ is the volumetric component). Negative values refer to shortening, and positive values refer to extension. The magnitude of the deviatoric strain tensor can be expressed as a scalar by the equivalent strain (Liu, 2005), defined as

$$\varepsilon_{eq} = \frac{2}{3}\sqrt{\frac{\left(\varepsilon_{11}-\varepsilon_{22}\right)^2+\left(\varepsilon_{22}-\varepsilon_{33}\right)^2+\left(\varepsilon_{33}-\varepsilon_{11}\right)^2+6\left(\varepsilon_{12}^2+\varepsilon_{13}^2+\varepsilon_{23}^2\right)}{2}}, \quad (1)$$

where $\varepsilon_{ij}$ (i, j = 1–3) are the components of the strain tensor. The stress tensor ($\sigma_{ij}$) is calculated from the strain tensor and the elastic stiffness constants ($C_{ijkl}$) (i,j,k,l = 1,3) for trigonal quartz (Ogi et al., 2006), by applying Hooke's law, $\sigma_{ij} = C_{ijkl}\,\varepsilon_{kl}$. Calculating orientation and strain tensor for each measured image allows preparation of maps that display their variations as a function of position. The spatial resolution of these maps is given by the scan step size (4 μm) and the diffraction volume. The inherent orientation resolution of <0.01° translates into a resolution of $<10^{-4}$ in strain tensor components. The resulting uncertainties in equivalent strain and equivalent stress are ~$10^{-4}$ and ~10 MPa, respectively (for more details, see the Data Repository).

## RESULTS

Detailed analyses of all four scans yielded similar results (see the Data Repository). We focus the discussion on one representative scan. Figure 1A shows the position of this scan within the petrographic thin section. Figure 1B shows a map of Euler orientation angle, Φ, which is the inclination of the crystal c-axis to the thin section. There is minor bending ~10° over the entire scan, with development of misoriented domains within the scanned area (<1°). The angles between the sharp Laue diffraction spots (Fig. 2), compared with ideal quartz, are reflecting the deviatoric elastic strain preserved in the quartz lattice and are used to compute equivalent strain $\varepsilon_{eq}$ (see Equation 1). The corresponding map of equivalent strain (Fig. 1C) indicates that strain is distributed somewhat heterogeneously within the scanned area, with coherent areas exceeding $2 \times 10^{-3}$ strain (orange red) and virtually strain-free areas (blue). The black cross in Figure 1C designates the position where the Laue pattern shown in Figure 2 was taken. Figure 3 shows maps of individual components of the elastic strain tensor along sample axes. The deviatoric linear x-component ($\varepsilon_{xx}$) (horizontal sample coordinate) is predominantly positive (yellow-orange), indicating extensional deformation along x, whereas the deviatoric y component ($\varepsilon_{yy}$) is predominantly negative (blue), indicating a compressional deformation parallel to y. The z-component, i.e., the one normal to the thin section surface, is close to zero (green), probably because much of the lattice strains normal to the thin section surface were released as it was cut. The crystal is divided into slightly misoriented domains (Fig. 1B), with some regions strain free (green) and others with residual elastic strain that was not released, due to local dislocations, disclinations, vacancies, and other defects (e.g., Kröner and Anthony, 1975; Cordier et al., 2014). A typical region is in the center of the scan (red for $\varepsilon_{xx}$ and blue for $\varepsilon_{yy}$).

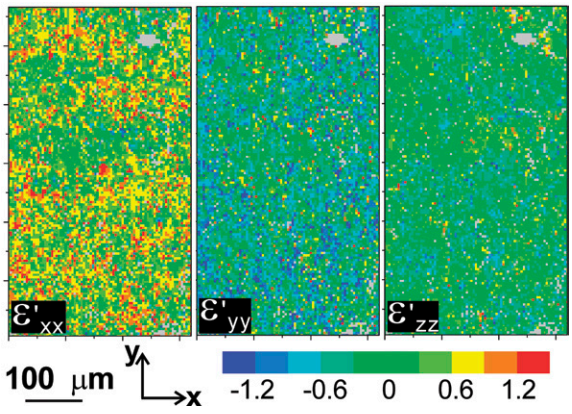


**Figure 3. Spatial distribution of individual strain components corresponding to the area depicted in Figure 1C. Negative values correspond to compressional strain, positive values represent extensional deformation. Deformations are predominantly extensional along the horizontal direction $\varepsilon_{xx}$ (red-yellow) and predominantly compressional (shortening) along the vertical direction $\varepsilon_{yy}$ (blue) (see text). Gray pixels indicate that the Laue patterns taken at these positions could not be indexed. Strain units are $10^{-3}$.**

The highest strains are ~ ±1.5 × $10^{-3}$ (Fig. 3). Figure DR1 (in the Data Repository) shows, for comparison, a scan over the synthetic quartz. This scan also shows some fluctuation in colors, but the magnitude (~±$10^{-4}$) is an order of magnitude lower than in the natural samples and within instrument resolution (<0.5 × $10^{-4}$). We conclude that the observed lattice strains in SAFOD quartz are not experimental or sample preparation artifacts.

### Strain and Stress Magnitude

The range and frequency of strain values measured in the SAFOD sample can be displayed in histograms and individual strain histograms. For all four scans on three grains (Fig. 4), these demonstrate similar strain distributions. Figure 5A shows the normalized equivalent strain histogram compiled from all four scans. The distribution peaks at 1 × $10^{-3}$, with a total range between 0.2 and >3 × $10^{-3}$. These values are lower bounds because Equation 1 treats all components equally and some of the strain normal to the sample surface has been released. The values are significantly above the inherent instrumental resolution measured on a strain-free synthetic quartz crystal, which shows a narrow distribution of equivalent strain of ~0.2 × $10^{-3}$ (Fig. 5A).

Deviatoric elastic strain values are the quantities measured in a Laue diffraction experiment. They can be converted to residual stress values, which are shown in Figure 5B. The equivalent stress peaks at ~130 MPa, with a range from 40 to 600 MPa. This is highly significant against the instrumental resolution of ~40 MPa measured on the synthetic quartz crystal.

## DISCUSSION

Residual stresses trapped in domains of quartz grains of cataclastic SAFOD samples are surprisingly high, and higher than previously reported macroscopic strengths for SAFOD samples. Carpenter et al. (2012) conducted shear experiments in a triaxial pressure vessel on samples from the SAFOD phase III core and found that the shear strength of rocks is ~10 MPa. A similar experiment by Lockner et al. (2011) found low coefficients of friction between 0.1 and 0.2, corresponding to shear strengths between 5 and 40 MPa. Stress drop values for San Andreas fault earthquakes between 24 and 63 MPa were estimated from seismic pulse frequencies and lengths (Harrington and Brodsky, 2009). Breakout strengths in an Integrated Ocean Drilling Program borehole (Expedition 343) indicate horizontal stresses of ~80 MPa and in-plane shear stresses of <2 MPa for the 2011 Tohoku-Oki Earthquake fault gouge (Lin et al., 2013).

Because of the long geological history of our sample, there are various events that are possibly responsible for the stress values recorded in in this work; they could be linked to the fragmentation of the source rock feeding the Great Valley Formation. We think this is unlikely because during fragmentation, erosion, and sediment transport the individual clastic components would have released any possible residual strain. A second possible origin is from stress fields associated with continuous creep within the San Andreas fault gouge. We consider this unlikely because slow creep in cataclastic rocks with a very weak matrix cannot sustain stresses exceeding the shear strength of quartz (~3 GPa) (LaLone and Gupta, 2009) in order to induce the observed brittle fracture. The most likely explanation is to attribute the observed high stress to seismic shock events. Such a mechanism can explain the high local strains observed in a matrix of weak phyllosilicates. Furthermore, the discrepancy between the macroscale and the microscale could be due to the heterogeneity of fault rocks. The sample is not fault gouge in the currently active zone, but nevertheless documents fracturing of rocks. The stress peaks in quartz were probably acquired during an earlier phase of the San Andreas fault history, and currently measured macrostrengths may not represent the original strength of rocks. Thus, in order to understand complex deformation such as seismicity, investigations at all scales are required.

It is interesting to compare our findings with similar measurements from a rock subjected to a meteor impact shock event. As can be seen

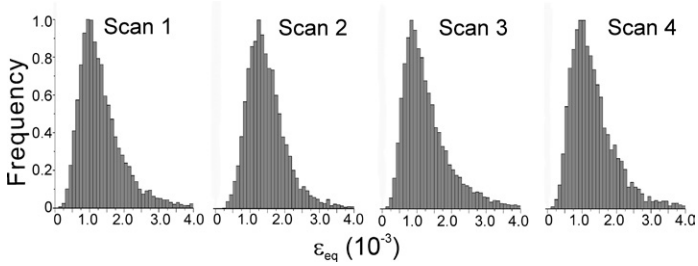


**Figure 4. Individual histograms normalized to the maximal bin for four scans performed on three different quartz grains within the same San Andreas Fault Observatory at Depth (SAFOD) sample. The composite of these scans is represented in Figure 5A. There are only minor variations between the scans, indicating that the phenomenon discussed herein is not an artifact of a unique grain, but rather a representative pattern within the SAFOD sample.**

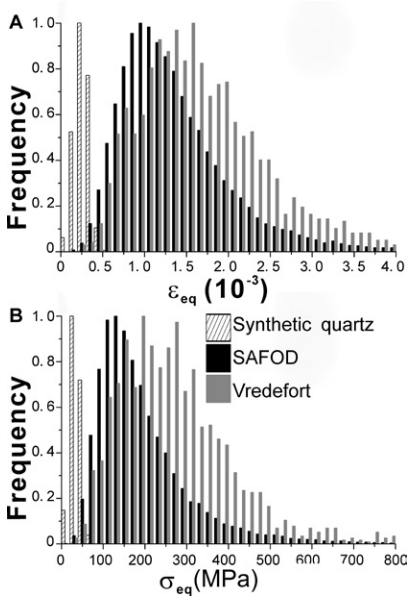


**Figure 5. Distribution histograms (see text). A: Equivalent strains (in $10^{-3}$). B: Equivalent stress (in MPa). The equivalent strain and stress distributions of a strain-free synthetic quartz, representing the experimental resolution, are compared with the average over four scans from San Andreas Fault Observatory at Depth (SAFOD) fault gouge (Fig. 4) and quartz from the Vredefort (South Africa) meteor impact crater (Chen et al., 2011).**

in the histograms in Figures 5A and 5B, elastic strains and stresses preserved in quartz from a stishovite-bearing quartzite from the Vredefort meteor crater in South Africa (Chen et al., 2011) are slightly higher than the SAFOD distributions (~1.4 × $10^{-3}$ strain and 200 MPa for Vredefort). Moreover, the Vredefort histograms show a broader distribution with large numbers of measurements past 4 × $10^{-3}$ strain and 500 MPa. This reflects that a larger shock stress was imposed on the meteor crater sample compared with the SAFOD sample subjected to a seismic shock wave. It is remarkable that such large amounts of residual strain were preserved for 2.0 b.y. in the Vredefort sample. In an earlier study of moderately deformed granite, lattice strain was much lower than that reported here, but still above that of a synthetic crystal (Kunz et al., 2009).

The fact that such high strains can be stored in a quartz grain for as long as billions of years is due to the strong confinement of the individual grain within the rock matrix. The heterogeneous distribution of the residual strain is believed to be related to local defects such as dislocations and vacancies.

This has been an exploratory study of cataclastic quartz from a fault zone. We have become aware of the potential of Laue X-ray microdiffraction to determine residual stress in minerals as a paleopiezometer. It gives us lower bound estimates because some stresses were obviously released during the geologic history and sample preparation. Nevertheless, we are impressed by the possibility of using this method not only to record stress intensities, but also stress directions in deformed rocks.

## CONCLUSION

We have been able to document residual stresses of >300 MPa in quartz in rocks extracted from SAFOD based on lattice strain measured with synchrotron X-ray microdiffraction. These are much higher values than average macroscopic stresses observed during seismic slip on fault surfaces, but lower than the actual shockwave that produced the comminution of macroscopic crystals into fragments. This result demonstrates the significance of scale for recording geological deformation processes.


## ACKNOWLEDGMENTS

The Advanced Light Source (ALS) is supported by the Director, Office of Science, Office of Basic Energy Sciences, Materials Science Division, of the U.S. Department of Energy under Contract DE-AC02-05CH11231 at Lawrence Berkeley National Laboratory. The microdiffraction program at the ALS on Beamline 12.3.2 was made possible by National Science Foundation grant 0416243. Chen is supported by the National Young 1000 Talents Program of China. Wenk acknowledges support from U.S. Department of Energy Basic Energy Sciences grant DE-FG02-05ER15637 and U.S. National Science Foundation grant EAR-1343908, Christoph Janssen for providing the sample, and help from Tim Teague in sample preparation. We are grateful for comments from reviewers and the editor that helped us to improve this presentation.


## REFERENCES CITED


Byerlee, J., 1978, Friction of rocks: Pure and Applied Geophysics, v. 116, p. 615–626, doi:10.1007/BF00876528.

Carpenter, B.M., Saffer, D.M., and Marone, C., 2012, Frictional properties and sliding stability of the San Andreas fault from deep drill core: Geology, v. 40, p. 759–762, doi:10.1130/G33007.1.

Chen, K., Tamura, N., Kunz, M., Tu, K.N., and Lai, Y.-S., 2009, In situ measurement of electromigration-induced transient stress in Pb-free Sn-Cu solder joints by synchrotron radiation based X-ray polychromatic microdiffraction: Journal of Applied Physics, v. 106, 023502, doi:10.1063/1.3157196.

Chen, K., Kunz, M., Tamura, N., and Wenk, H.-R., 2011, Evidence for high stress in quartz from the impact site of Vredefort, South Africa: European Journal of Mineralogy, v. 23, p. 169–178, doi:10.1127/0935-1221/2011/0023-2082.

Chen, K., Dejoie, C., and Wenk, H.R., 2012, Unambiguous indexing of trigonal crystals from white-beam Laue diffraction patterns: Application to Dauphiné twinning and lattice stress mapping in deformed quartz: Journal of Applied Crystallography, v. 45, p. 982–989, doi:10.1107/S0021889812031287.

Chester, F.M., et al., 2013, Structure and composition of the plate-boundary slip zone for the 2011 Tohoku-Oki earthquake: Science, v. 342, p. 1208–1211, doi:10.1126/science.1243719.

Cordier, P., Demouchy, S., Beausir, B., Taupin, V., Barou, F., and Frassengeas, C., 2014, Disclinations provide the missing mechanism for deforming olivine-rich rocks in the mantle: Nature, v. 507, p. 51–56, doi:10.1038/nature13043.

Gratier, J.P., Richard, J., Renard, F., Mittempergher, S., Doan, M.L., Di Toro, G., Hadizadeh, J., and Boullier, A.M., 2011, Aseismic sliding of active faults by pressure solution creep: Evidence from the San Andreas Fault Observatory at Depth: Geology, v. 39, p. 1131–1134, doi:10.1130/G32073.1.

Harrington, R.M., and Brodsky, E.E., 2009, Source duration scales with magnitude differently for earthquakes on the San Andreas fault and on secondary faults in Parkfield, California: Seismological Society of America Bulletin, v. 99, p. 2323–2334, doi:10.1785/0120080216.

Ice, G.E., Budai, J.D., and Pang, J.W., 2011, The race to X-ray microbeam and nanobeam science: Science, v. 334, p. 1234–1239, doi:10.1126/science.1202366.

Janssen, C., Kanitpanyacharoen, W., Wenk, H.R., Wirth, R., Morales, L., Rybacki, E., Kienast, M., and Dresen, G., 2012, Clay fabrics in SAFOD core samples: Journal of Structural Geology, v. 43, p. 118–127, doi:10.1016/j.jsg.2012.07.004.

Jiang, T., Wu, C., Spinella, L., Im, J., Tamura, N., Kunz, M., Son, H.-Y., Gyu Kim, B., Huang, R., and Ho, P.S., 2013, Plasticity mechanism for copper extrusion in through-silicon vias for three-dimensional interconnects: Applied Physics Letters, v. 103, 211906, doi:10.1063/1.4833020.

Kröner, E., and Anthony, K.-H., 1975, Dislocations and disclinations in materials structures: The basic topological concepts: Annual Review of Materials Research, v. 5, p. 43–72, doi:10.1146/annurev.ms.05.080175.000355.

Kunz, M., et al., 2009, A dedicated superbend x-ray microdiffraction beamline for materials, geo-, and environmental sciences at the advanced light source: Review of Scientific Instruments, v. 80, 035108, doi:10.1063/1.3096295.

LaLone, B.M., and Gupta, Y.M., 2009, Elastic limit of x-cut quartz under shockless and shock wave compression: Loading rate dependence: Journal of Applied Physics, v. 106, 053526, doi:10.1063/1.3213369.

Lin, W., Conin, M., Moore, J.C., Chester, F.M., Nakamura, Y., Mori, J.J., Anderson, L., Brodsky, E.E., Eguchi, N., and Expedition 343 Scientists, 2013, Stress state in the largest displacement area of the 2011 Tohoku-Oki earthquake: Science, v. 339, p. 687–690, doi:10.1126/science.1229379.

Liu, A.F., 2005, Mechanics and mechanisms of fracture: An introduction: Materials Park, Ohio, ASM International, 654 p.

Lockner, D.A., Morrow, C., Moore, D., and Hickman, S., 2011, Low strength of deep San Andreas fault gouge from SAFOD core: Nature, v. 472, p. 82–85, doi:10.1038/nature09927.

Ma, K.F., et al., 2006, Slip zone and energetics of a large earthquake from the Taiwan Chelungpu-fault Drilling Project: Nature, v. 444, p. 473–476, doi:10.1038/nature05253.

Noyan, I.C., and Cohen, J.B., 1987, Residual stress: Measurement by diffraction and interpretation: New York, Springer-Verlag, 276 p.

Ogi, H., Ohmori, T., Nakamura, N., and Hirao, M., 2006, Elastic, anelastic, and piezoelectric coefficients of α-quartz determined by resonance ultrasound spectroscopy: Journal of Applied Physics, v. 100, 053511, doi:10.1063/1.2335684.

Ohtani, T., Fujimoto, K., Ito, H., Tanaka, H., Tomida, N., and Higuchi, T., 2000, Fault rocks and past to recent fluid characteristics from the borehole survey of the Nojima fault ruptured in the 1995 Kobe earthquake, southwest Japan: Journal of Geophysical Research, v. 105, p. 16,161–16,171, doi:10.1029/2000JB900086.

Tamura, N., 2014, XMAS: A versatile tool for analyzing synchrotron X-ray microdiffraction data, *in* Ice, G.E., and Barabash, R., eds., Strain and dislocation gradients from diffraction: London, Imperial College Press, p. 125–155.

Townend, J., Sutherland, R., and Toy, V., 2009, Deep Fault Drilling Project—Alpine fault, New Zealand: Scientific Drilling, v. 8, p. 75–82, doi:10.5194/sd-8-75-2009.

van der Elst, N.J., and Brodsky, E.E., 2010, Connecting near-field and far-field earthquake triggering to dynamic strain: Journal of Geophysical Research, v. 115, B07311, doi:10.1029/2009JB006681.

Xue, L., et al., 2013, Continuous permeability measurements record healing inside the Wenchuan earthquake fault zone: Science, v. 340, p. 1555–1559, doi:10.1126/science.1237237.

Zoback, M., Hickman, S., and Ellsworth, W., 2011, Scientific drilling into the San Andreas fault zone—An overview of SAFOD's first five years: Scientific Drilling, v. 11, p. 14–28, doi:10.5194/sd-11-14-2011.



Manuscript received 11 November 2014
Revised manuscript received 17 December 2014
Manuscript accepted 18 December 2014

Printed in USA